Physica B 500 (2016) 118–125

Contents lists available at ScienceDirect

Physica B

journal homepage: www.elsevier.com/locate/physb

Magneto-transport properties of As-implanted highly oriented pyrolytic graphite

R.F. de Jesus [a], B.C. Camargo [b], R.R. da Silva [b], Y. Kopelevich [b], M. Behar [a], M.A. Gusmão [a], P. Pureur [a,*]

[a] Instituto de Física, Universidade Federal do Rio Grande do Sul, P.O. Box 150151, 91501-970 Porto Alegre, RS, Brazil
[b] Instituto de Física Gleb Wathagin, Universidade Estadual de Campinas, UNICAMP, 13083-970 Campinas, SP, Brazil

ARTICLE INFO

Article history:
Received 27 May 2016
Received in revised form
21 July 2016
Accepted 22 July 2016
Available online 25 July 2016

Keywords:
Highly oriented pyrolytic graphite
Ion implantation
Magneto-resistance
Hall effect
Shubnikov-de Haas oscillations

ABSTRACT

We report on magneto-transport experiments in a high-quality sample of highly-oriented pyrolytic graphite (HOPG). Magneto-resistance and Hall resistivity measurements were carried out in magnetic inductions up to $B = 9$ T applied parallel to the c-axis at fixed temperatures between $T = 2$ K and $T = 12$ K. The sample was submitted to three subsequent irradiations with As ions. The implanted As contents were 2.5, 5 and 10 at% at the maximum of the distribution profile. Experiments were performed after each implantation stage. Shubnikov-de Haas (SdH) oscillations were observed in both the magneto-resistance and Hall-effect measurements. Analyses of these results with fast Fourier transform (FFT) lead to fundamental frequencies and effective masses for electrons and holes that are independent of the implantation fluences. The Hall resistivity at low temperatures shows a sign reversal as a function of the field in all implanted states. We interpret the obtained results with basis on a qualitative model that supposes the existence of an extrinsic hole density associated to the defect structure of our sample. We conclude that the As implantation does not produce a semiconductor-type doping in our HOPG sample. Instead, an increase in the extrinsic hole density is likely to occur as a consequence of disorder induced by implantation.

1. Introduction

Carbon-based materials in different allotropic forms have attracted much attention over the years because of the large variety of their physical properties, as well as to the great importance of their technological applications. For sp^2 hybridization, the solid carbon structure is known as graphite. This system may be viewed as a stack of weakly coupled graphene atomic planes [1]. Depending on the stacking sequence of the layers, graphite can have three types of stacking: a simple hexagonal AAA-stacking [2], the most common Bernal ABA-stacking [3], and the ABC-stacking [4].

The electronic properties of ABA graphite have been first studied by Wallace [5], who showed that neglecting out-of-plane interactions, the system behaves as a zero-gap semiconductor. Later on, using the $k.p$ method and treating the out-of-plane interactions as a perturbation, Slonczewski and Weiss [6] proposed a 3D band model, nowadays known as the Slonczewski-Weiss model (SW), which is based on seven phenomenological hopping parameters. These authors concluded that graphite is a semi-metal with a small band overlap along the H-K-H edge of the hexagonal first Brillouin zone [6]. Analyzing results obtained from de Haas–van Alphen oscillations [7], McClure [8] showed that the band overlap is about 0.03 eV, contrasting with the value $\gamma_1 \sim 0.3$ eV predicted by the SW-model. This author also showed that carriers with low effective masses give origin to a small Fermi surface (FS) formed by elongated pockets of electrons and holes ordered successively along the H-K-H edge. Recent results on the electronic structure of graphite obtained from ARPES measurements in Bernal-type samples [9] are in good agreement with the theoretical predictions of the SW-model and the experimental analysis by McClure.

Carrier properties such as small FS, low density, small effective masses, and large mean free path lead graphite to reach the Landau-level quantization condition in rather low applied magnetic fields when compared to usual metallic systems [10]. Quantum phenomena such as Shubnikov-de Haas effect (SdH) in magneto-transport properties [11,12], de Haas-van Alphen effect in magnetization [7,13,14], quantum Hall effect [15–17] and oscillatory Nernst effect [18,19] have been observed in highly oriented pyrolytic graphite (HOPG) and natural single-crystal graphite in magnetic inductions as low as $B = 1$ T . Concerning the experimental study of quantum phenomena in graphite an

* Corresponding author.
E-mail address: ppureur@if.ufrgs.br (P. Pureur).

http://dx.doi.org/10.1016/j.physb.2016.07.027
0921-4526/

interesting approach is to explore the possibility of doping this system in order to modulate its FS. Along this line of investigation, the tuning of the electronic properties of HOPG has been attempted by means of ionic implantation [20–24] and proton or neutron irradiation [25,26]. While inconclusive with respect to doping, these studies revealed that the weak ferromagnetic response of graphite observed when the magnetic field is oriented parallel to the graphene planes is enhanced by defects and vacancies created by irradiation [25,27–29].

In this work we report on magneto-transport experiments in a HOPG sample implanted with As ions at different fluences. In these experiments, the magnetic field was applied perpendicular to the graphene layers. We find that the Hall resistivity and the planar magneto-resistance amplitude vary significantly with the content of implanted As ions. Moreover, superimposed to the Boltzmann-type charge transport, quantum oscillations in magneto-resistance (MR) as well as in the Hall effect (HE) were observed. The fundamental frequencies could be estimated from analysis of the results with fast Fourier transform (FFT) and were found to be independent of the As content. Cyclotron effective masses were estimated from the amplitudes of the peaks for each measured temperature by using the thermal damping factor of the Lifshitz-Kosevich (LK) theory [30]. We discuss the possibility for the occurrence of As doping in the graphene planes of graphite. Our results are discussed taking into account the apparently contradictory outcomes obtained from the Boltzmann-type electrical conduction and the quantum effects in the magneto-transport properties of our As-implanted graphite.

2. Experimental

A highly oriented sample of pyrolytic graphite was cut out from a pellet sourced by the Great Wall Company. The full widths at half-maximum (FWHM) of the studied HOPG is 0.39 degrees [31]. The sample has dimensions $3.2 \times 1.5 \times 0.26$ mm. In the pristine state, the sample is labeled GW-Pure. The magneto-transport properties of this specimen were studied previously to the implantation processes, so that GW-Pure is considered as a reference sample. The same HOPG piece was submitted to three subsequent As implantations on one of its largest faces. The fluence for the first implantation process was 0.25×10^{16} ions/cm^2. The As content attained 2.5 at% at the center of the implantation profile. This state of the sample is labeled GW-As (0.25). After completion of the magneto-transport measurements, this same piece was further implanted until the accumulated fluence was 0.5×10^{16} ions/cm^2 and the As concentration reached 5 at%. In this state the sample is named GW-As (0.5). Measurements were then repeated. In third process the attained fluence was 1.0×10^{16} ions/cm^2 and the total As concentration attained 10 at% at the peak of the implantation profile. In this case, the sample is named GW-As (1.0). Magneto-transport experiments were performed in this case as well.

The condition $\hbar\omega_B \gg k_B T$, where ω_B is the cyclotron frequency, can be easily satisfied for graphite at low temperatures. However, the condition $\omega_B \tau \gg 1$, where τ is the transport relaxation time, may not be fulfilled even at $T=0$. When both conditions are satisfied, it is possible to study quantum effects in the magneto-transport properties of graphite using a conventional superconductor solenoid. We then perform magneto-resistance and Hall-effect measurements using a commercial Quantum Design PPMS® system at the fixed temperatures $T=2$ K, 3 K, 5 K, 7 K and 12 K as functions of the magnetic field that was changed in the range between -9 T $\leq B \leq$ 9 T. The temperature dependent electrical resistivity at zero applied field was also measured between 2 K and 300 K. Measurements were carried out with the AC technique option using a 1 mA current. Six electrical contacts were deposited with silver paste on the sample surface oriented parallel to the graphene planes, as shown in the upper insert of Fig. 1. Gold wires were attached to these contacts. For the Hall voltage detection, contacts placed on opposite edges of the sample surface were used. For the resistivity and magneto-resistance experiments, the contacts for current and voltage were aligned. This same surface was exposed to As implantation. Since the thickness of the GW piece is much larger than the penetration depth of the implanted ions, special care was taken to dispose the electrical contacts exclusively on the irradiated surface in order to detect appreciable effects from implantation in the magneto-transport measurements. Due to the huge anisotropy of the electrical transport in HOPG [32,33], we assume that placing the current contacts close to each other and the voltage contacts in-between ensures that a large fraction of the current intensity probes the superficial implanted region. Detailed studies of the spreading resistance in HOPG using circular metallic contacts of nanometric size justify this assumption [33].

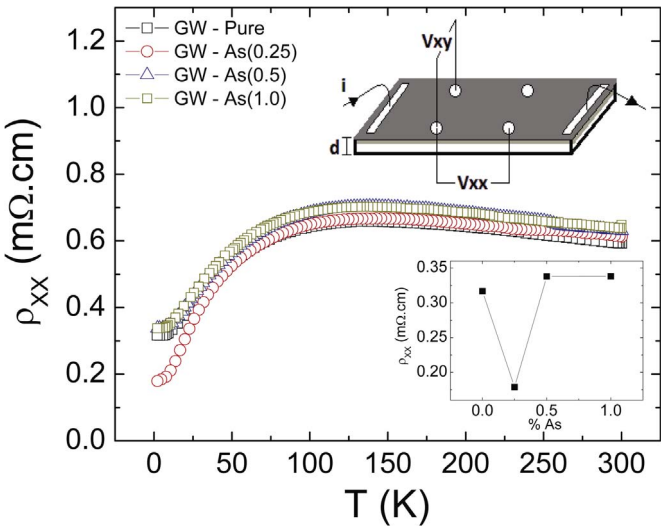

Fig. 1. Longitudinal resistivity versus temperature in the HOPG-GW sample for all studied fluences. Upper insert: electrical contact configuration; V_{XX} and V_{XY} are the longitudinal and transversal voltage, respectively. The implanted region is represented by the grayish upper layer. Lower inset: residual resistivity measured at $T=2$ K for different fluences.

The implantations were carried out with the 500 keV Ion Implanter of the Instituto de Física, UFRGS. The ionic implantation parameters were obtained from the software Stopping and Range of Ions in Matter (SRIM) which is based on Monte Carlo statistical simulation [34]. The distribution of the implanted atoms has a Gaussian profile with center 16.4 nm below the irradiated surface and 3.6 nm straggling. Table 1 list the relevant implantation parameters used in this study.

Table 1
Parameters for As implantation in HOPG.

Parameters	Sample		
Procedure	Step 1	Step 2	Step 3
Current (nA)	50	50	120
Energy (KeV)	20	20	20
Fluence[a] (1016 cm^{-2})	0.25	0.50	1.00
Temperature (°C)	30	30	30
Depth[b] (nm)	16.4	16.4	16.4
Straggling (nm)	3.6	3.6	3.6
Concentration (%)	2.5	5	10
Sample label	GW-As (0.25)	GW-As (0.50)	GW-As (1.00)

[a] Nominal accumulated fluence at the maximum of implanted distribution.
[b] Gaussian profile.

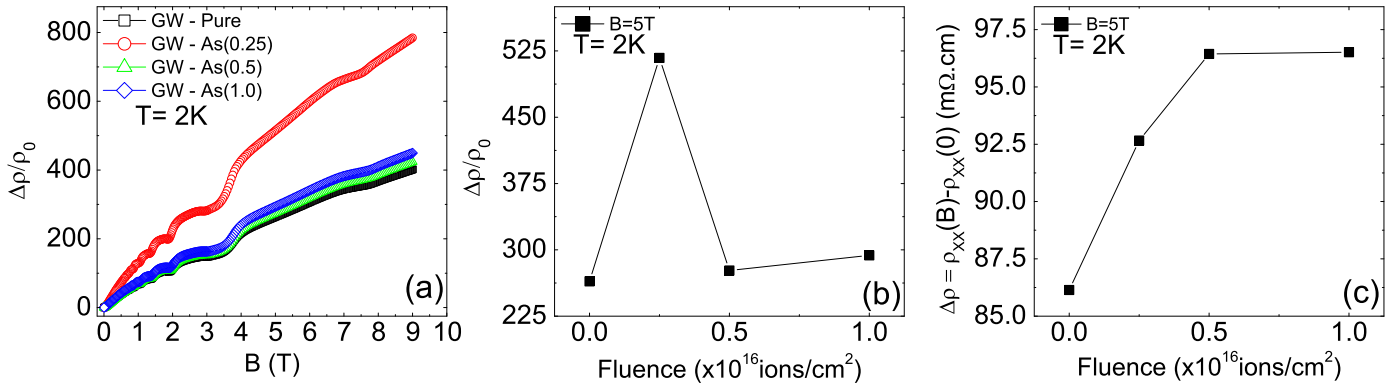

Fig. 2. a) Normalized magneto-resistance for the HOPG-GW sample measured at $T=2$ K as a function of the magnetic field for all fluences, as indicated. (b) Reduced magneto-resistance measured in $B=5$ T and $T=2$ K as a function of the fluence. (c) As in panel (b), but for the non-normalized MR, $\Delta\rho = \rho_{xx}(B) - \rho_{xx}(0)$.

In order to keep the background quenched disorder intact, the samples were not annealed at high temperatures before performing the magneto-transport measurements.

3. Results and discussion

In the magneto-transport experiments carried out in this work the magnetic field was kept parallel to the *c*-axis of the HOPG sample, while the current was applied parallel to the graphene planes. The normalized MR is defined as $\Delta\rho_{xx}/\rho_0 = \left[R_{xx}(B) - R_{xx}(0)\right]/R_{xx}(0)$, where the longitudinal resistance $R_{xx}(B)$ is measured in the presence of the magnetic induction B. The Hall resistivity was obtained from the average of the transversal resistance at positive and negative fields as $\rho_{xy} = [R_{xy}(B) - R_{xy}(0)]d/2$, where d is the sample thickness. This method for measuring the Hall effect was adopted to eliminate any spurious signal due to the longitudinal resistivity caused by unavoidable misalignment of the Hall contacts. We remark that presenting the MR and Hall resistivity data in terms of the globally measured longitudinal and Hall resistances is a just practical procedure useful for quantitatively comparing results obtained from samples cut from different pieces of the original HOPG pellet. In fact, the reported absolute values for ρ_{xx} and ρ_{xy} are non-trivially related to parallel associations of resistances and Hall voltages that are pertinent to a sample formed by a thin region modified by ion irradiation lying above pristine HOPG where the current flow is non homogeneous because of the adopted electrical contact configuration.

3.1. Longitudinal resistivity

Fig. 1 shows the temperature dependence of the longitudinal resistivity measured in the studied GW-HOPG sample for all implantation fluences. From room temperature down to about 140 K the sample has a semiconductor-like behavior, regardless of the implantation. Subsequent irradiations produce small increments in the resistivity magnitude at high temperatures. A crossover to a metallic-like behavior is observed at low temperatures. It is well-known that commercial HOPG and single-crystal graphite may have a semiconductor and/or metallic-like behavior according to the origin of the sample and conditions for its preparation [35]. Different morphological features produce qualitative and quantitative modifications in the electrical transport properties of graphite [35]. The growth temperature of HOPG samples also influences the resistivity of this system [36], probably because of changes on the energy bands related to the heat-treatment temperature [37]. The crossover from $d\rho_{xx}(T)/dT < 0$ to $d\rho_{xx}(T)/dT > 0$ has been associated to the pronounced two-dimensional character of the electronic conduction in graphite [38]. Alternatively, this crossover can be accounted for by competing contributions of the electron and hole carrier densities and their respective mobility [36].

A relevant feature in the results of Fig. 1 is the significant decrease of the residual resistivity (measured at $T=2$ K) in GW-As (0.25). The inset in Fig. 1 shows the variation of the residual resistivity as a function of the implantation fluence. The decrease of the residual resistivity for the GW-As(0.25) state is of unknown origin, but is undoubtedly an effect of implantation. A possibility is that the point defects (vacancies) produced in low fluences give origin to less resistive channels for planar electron conduction. At higher fluences, defects as vacancy complexes and amorphization may prevail, destroying the highly conductive channels.

3.2. Magneto-resistance

Fig. 2(a) shows the planar magneto-resistance measured at $T=2$ K with field applied perpendicular to the graphene planes for all implantation states. In the pristine state (GW-Pure), the MR amplitude reaches $(\Delta\rho/\rho_0) \approx 400$ at the maximum induction, $B = 9$ T. This amplitude is two times larger in GW-As (0.25). The MR amplitude in the subsequent implanted states increases slightly with respect to that for GW-Pure and varies proportionally to the fluence. Fig. 2(b) shows the reduced MR in $B=5$ T and $T=2$ K as a function of the fluence. The pronounced maximum observed for GW-As (0.25) is mostly due to the smaller resistance at zero field for this state of the sample. Fig. 2(c) shows the non-normalized magneto-resistance measured at the same field and temperature as in panel (b). There one observes that a small but steady increase of $\Delta\rho(B=5T)$ occurs when the fluence is increased up to 0.5×10^{16} ion/cm^2, then becoming constant with further fluence augmentation. This behavior is similar to that previously observed in Na-implanted HOPG [29] and suggests that the As implantation produces small modifications in the electronic properties of graphite.

Extremely large MR is a common characteristic of compensated semimetals with high mobility carriers as Bi [39–42], Cd_3As_2[43,44], NbP [45], and WTe_2[46]. The origin of the giant magneto-resistance in graphite is often considered as a Lorentz force effect in a two-band conducting system with rather small effective mass carriers [47]. This mechanism, however, predicts a MR saturation in the high field limit, $\omega_B\tau \gg 1$. Usually, one considers that this limit in graphite is reached for fields $B \geq 1$ T, since SdH quantum oscillations in MR are detectable at this field magnitude. The absence of any tendency to MR saturation in our graphite sample, even when the applied field is close to its maximum value,

might be taken as an indication that a significant fraction of the carriers in this system propagates with rather short relaxation time. Other interpretations may be found for the ever increasing MR of graphite. For instance, it was recently proposed that the large and almost linearly field dependent MR in graphite is due to a time-reversal symmetry breaking effect that quenches or confines excitations that are responsible for both the electrical transport in the graphene planes and the strong diamagnetic signal observed in response to magnetic fields applied perpendicularly to these planes [48].

Fig. 2(a) shows that the MR oscillations in graphite cease for fields around $B=8$ T, where the quantum limit is reached for the electron-type carriers. The quantum limit for hole carriers is expected to occur at a lower field value [49,50].

The standard LK theory for quantum oscillations in the MR predicts that

$$\frac{\Delta\rho}{\rho_0} \propto R_T R_D R_S \cos\left[2\pi\left(\frac{F}{B}-\gamma\right)\right]. \quad (1)$$

Terms appearing in Eq. (1) are: (i) R_T is the temperature damping factor, given as $R_T = (\kappa a T/B)/\sinh(\kappa a T/B)$, where $\kappa = 14.7$ T/K is a constant, and $a = m^*/m_e$ is the effective mass normalized to the free electron mass; (ii) R_D is the Dingle factor [51], given by $R_D = \exp(-aT_D/B)$, where T_D denotes the Dingle temperature; (iii) R_S is the spin-splitting dependence of the amplitude oscillation, $R_S = \cos(-\pi g a/2)$, where g is the Landé factor; (iv) F is the fundamental frequency; and (v) γ is a phase factor, $0 \le \gamma \le 1$.

We analyze the SdH oscillations in the magneto-resistance in terms of the numerically determined second derivative, $d^2\rho_{xx}/dB^2$, so that the contribution of the monotonic contribution to the MR is largely suppressed. In Fig. 3(a), we plot d^2R_{xx}/dB^2 obtained from measurements carried out at $T=2$ K as a function of $1/B$ for all implanted states. Similar results were obtained for the other studied temperatures, though a significant broadening of the oscillation spectrum occurs for $T \ge 4$ K. Fig. 3(a) clearly shows that the relevant range of magnetic fields for observing SdH oscillations in graphite is limited to $0.25\ T^{-1} < B^{-1} < 2.5\ T^{-1}$.

The results shown in Fig. 3(a) were analyzed by fast Fourier transform (FFT). The outcome of this analysis is shown in Fig. 3(b). The observed peaks correspond to two distinct fundamental frequencies and their first harmonic. The results in Fig. 3(b) are in a good agreement with previous determinations of the fundamental oscillation frequencies in graphite, including those obtained using other techniques [32]. With basis on the Onsager relation [52], $F = (\hbar/2\pi e)S_{extr}$, which states that the frequency of the quantum oscillations is proportional to an extreme area of the Fermi surface, it has been shown that the lowest frequency, $F_h \simeq 4.6$ T , corresponds to the hole pocket of the FS, whereas $F_e \simeq 6.4$ T is associated to the electron pocket [12].

Results in Fig. 3(b) do not hint at the occurrence of shifts induced by As implantation in the fundamental frequencies of SdH oscillations in our GW-HOPG graphite. This fact does not rule out completely the possibility for the existence of some doping produced by the implanted ions. However, such an effect would not be significant enough to change the extreme areas of the FS. We notice that experiments similar to ours, but using proton irradiation were performed in a high quality HOPG sample (ZYA grade, 0.40 mosaic spread) [25]. This study also does not reveal appreciable carrier-doping effects for fluences up to $10^{16}/cm^2$. Only for a fluence as high as $10^{17}/cm^2$ the effects of proton irradiation on the quantum oscillations were reported to become appreciable [25].

Fig. 4(a) shows the FFT analyses carried out for all implanted states in several temperatures. One clearly observes that the values for the hole (F_h) and electron (F_e) frequencies do not change with temperature. This behavior shows that the extreme areas of the FS are temperature independent in the low-T regime. Fig. 4 (b) displays the amplitudes of the FFT peaks for holes and electrons plotted as a function of temperature. These amplitudes were fitted to the thermal damping factor R_T of the LK theory, as given by (1). The fittings allowed us to estimate the carriers' effective masses for the studied fluences, as listed in Table 2.

Table 2 shows that the effective masses for both holes and electrons remain constant upon implantation in our GW-HOPG. Moreover, the listed values of effective masses are in accordance to those reported in the literature for pure graphite [32]. Thus, the study the SdH oscillations in our sample does not reveal sizable modifications produced by As implantation in the electronic properties of graphite.

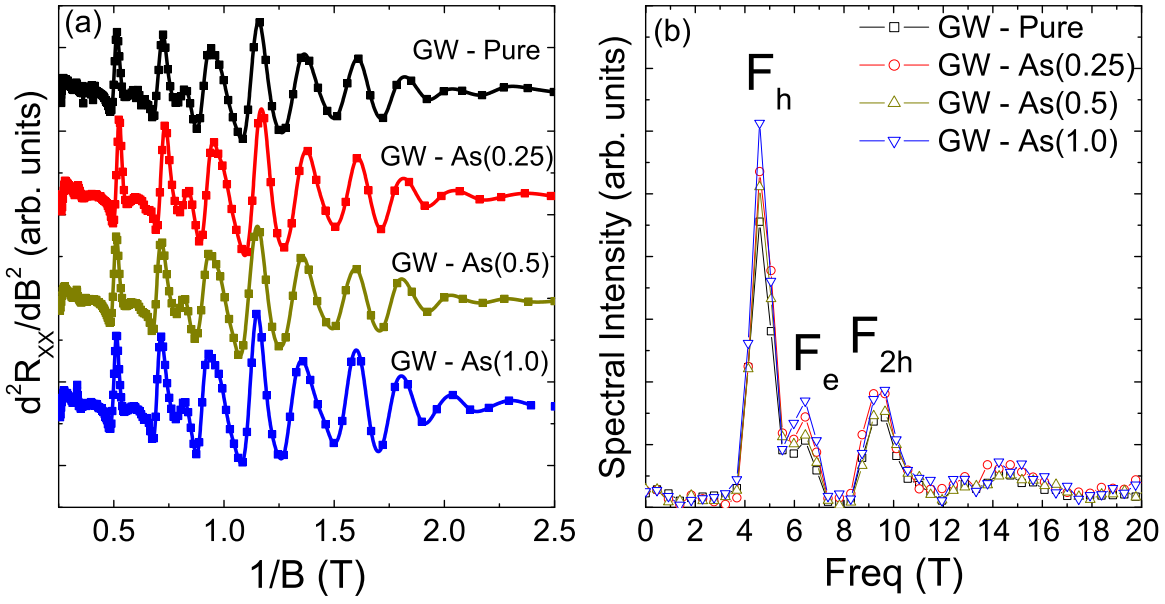

Fig. 3. (a) Second derivative $d^2\rho_{xx}/dB^2$ versus B^{-1} for GW–Pure, GW-As (0.25), GW-As (0.5) and GW-As (1.0) determined at $T=2$ K. The curves are shifted vertically for clarity. (b) Fast Fourier transform (FFT) of the data plotted in (a), indicating the relevant frequencies.

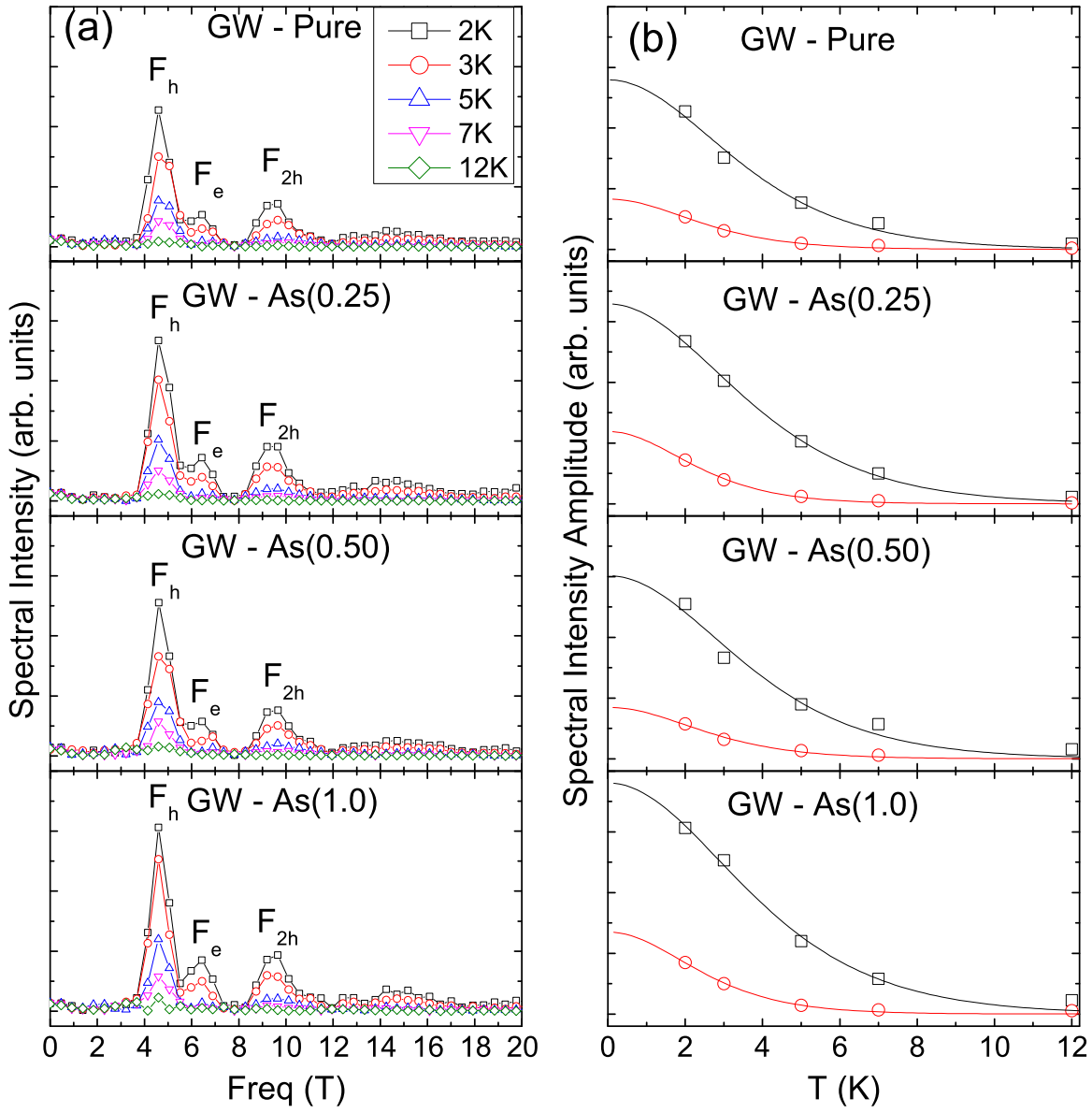

Fig. 4. (a) Spectral intensity obtained from the FFT analyses of the oscillatory MR component in our GW sample for the studied implantation states. Data were obtained in the quoted temperatures. (b) Fittings of the FFT peaks amplitude to the thermal damping factor of the LK theory. Squares (black) correspond to the hole frequency F_h and open circles (red) to the electron frequency F_e. (For interpretation of the references to color in this figure legend, the reader is referred to the web version of this article.)

Table 2
SdH fundamental frequencies and effective masses for the GW-HOPG sample in different implantation states.

Sample	F_h [a]	Hole effective mass	F_e [b]	Electron effective mass
GW-Pure	4.59	0.029	6.43	0.046
GW-As(0.25)	4.59	0.029	6.43	0.047
GW-As(0.5)	4.59	0.030	6.43	0.041
GW-As(1.0)	4.59	0.028	6.43	0.044

[a] Fundamental frequency for hole carriers.
[b] Fundamental frequency for electron carriers.

3.3. Hall effect

Fig. 5(a) shows the Hall resistivity as a function of the applied field for all As-implanted states of our HOPG-GW sample at $T=2$ K. Contrasting with the longitudinal magneto-resistance, the Hall resistivity is strongly dependent on the As implantation. Also remarkable is the sign reversal that occurs in ρ_{xy} at characteristic applied fields $B^* \simeq 7$ T in the pristine sample and $B^* \simeq 4$ T in the implanted states. Qualitatively distinct Hall effect results have been reported for graphite to which different interpretations have been proposed [53–56]. The remarkable differences among the HE results reported for graphite indicates that this property depends crucially on extrinsic morphological aspects of the sample. Likely, this is also the case for resistivity, magneto-resistance and the SdH oscillation amplitude. Concerning the results in Fig. 5, it appears that in applied fields below B^* the Hall resistivity behaves approximately as predicted by the two-band model for Boltzmann-type transport to which SdH quantum oscillations are superimposed.

Within the two-band model, the Hall resistivity varies non-linearly with the applied field, except in the asymptotic low ($\omega_B\tau \ll 1$) and high ($\omega_B\tau \gg 1$) field limits. In low fields this model predicts that the Hall resistivity is given by [57]

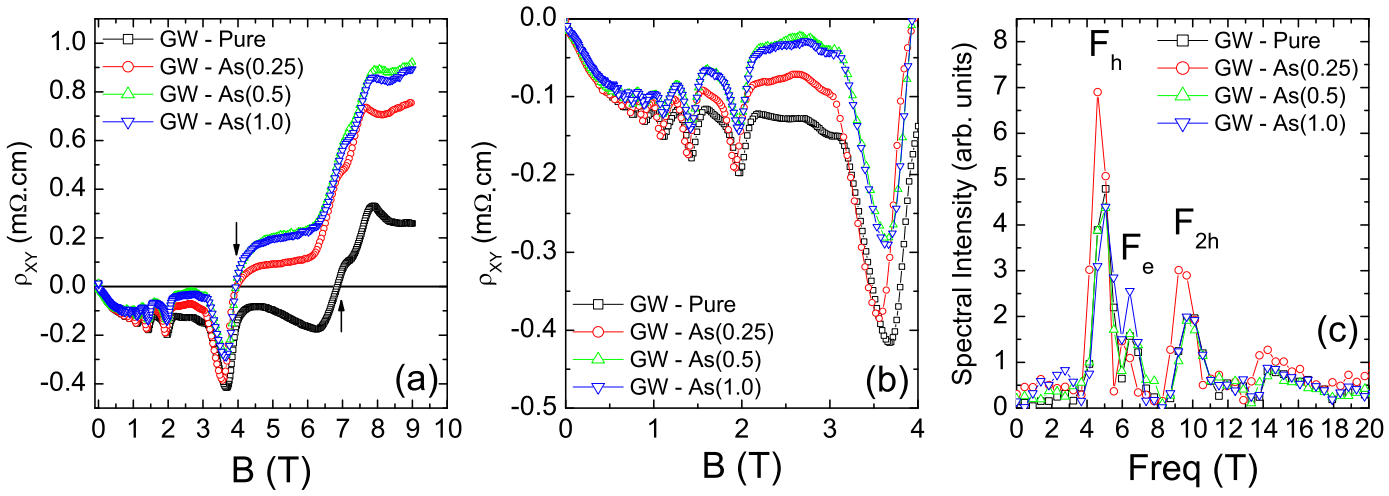

Fig. 5. (a) Hall resistivity ρ_{xy} measured at T=2 K plotted as a function of magnetic field for all implantation states. Vertical arrows denote the position of B^* ($B^* = 7$ T for the pure sample; $B^* = 4$ T for the implanted samples) (b) The same case as in (a) but for the field region where most of the quantum oscillations occur. (c) Fast Fourier transform of the data in (b).

$$\rho_{xy} = \frac{1}{e}\frac{n_h\mu_h^2 - n_e\mu_e^2}{(n_h\mu_h + n_e\mu_e)^2}B, \tag{2}$$

where e is the absolute value of the electron charge, $n_{h(e)}$ and $\mu_{h(e)}$ are the density and mobility of hole (electron) carriers, respectively. According to results in Fig. 5(a), in very low applied fields the Hall constant R_H is negative and practically independent of the As implantation. Supposing that R_H is entirely due to electrons in this field limit, one calculates $n_e \geq 2.8 \times 10^{18}$ cm $^{-3}$ using Eq. (2) with $n_h = 0$. This value is in fairly good agreement with other estimations for the electron density in graphite [53].

Above $B \simeq 0.3$ T, the Boltzmann-type contribution to the Hall resistivity deviates from linearity. For $B \geq 0.5$ T, quantum oscillations become increasingly discernible, in agreement with the MR data. Above this field, the deviation of $\rho_{xy}(B)$ towards positive values is enhanced for larger fluences. The Hall resistivity becomes positive above $B^* \simeq 7$ T for GW-Pure and $B^* \simeq 4$ T for the implanted states. The change of the Hall signal is not an universal characteristic of all commercial graphite samples, though this feature was observed previously [12,49,58]. In our sample, $\rho_{xy}(B)$ increases continuously up to highest applied field above the sign reversal. In the results of Fig. 5(a), one observes that quantum SdH oscillations of large amplitude are superimposed to an approximately quadratic behavior of $\rho_{xy}(B)$ in the high-field range. Analyses of the SdH oscillations using the Hall resistivity data were carried out by performing derivatives as in the case of magneto-resistance. Most of the relevant oscillations occur in the field range between 0.5 T $\leq B \leq$ 4 T. As shown in Fig. 5(b), FFT analysis of the oscillatory contribution to $\rho_{xy}(B)$ leads to the same fundamental frequencies obtained previously from the MR results. These frequencies do not shift visibly upon As-implantation. In the highest applied fields, the observed shoulders in $\rho_{xy}(B)$ are related to spin-splitting of the lowest Landau level for the electron pocket [59].

Eq. (2) offers a simple scenario to understand the overall behavior of the non- oscillatory contribution to the ρ_{xy} results in Fig. 5, provided that a significant fraction of the hole carrier density is not submitted to Landau quantization. These extrinsic holes might come from a narrow band related to defect structures in HOPG, and their contribution to the hole density is probably sample dependent. In the specific case of our sample, the ion implantation is a source for defects, since it generates structural damage and may induce amorphization in the superficial atomic layers of graphite [60]. Charge transport by the extrinsic hole carriers should be present in the whole studied field range. In the proposed model, the deviations of $\rho_{xy}(B)$ towards positive values as the field magnitude continuously increases and the subsequent sign reversal can be understood as consequences of the decrease in the electron density n_e available for Boltzmann-type transport caused by condensation of electron carriers into Landau levels. The electron density should be reduced upon field increase at least until the lowest Landau level quantization is attained for electron carriers around $B \simeq 9$ T [50]. The same condensation into quantized orbits must occur for intrinsic holes having low effective mass, but without affecting too much the total hole density n_h, so that the numerator of Eq. (2) eventually becomes positive at some value of the applied field. At this point one might also consider the possibility for the occurrence of a magnetic freezing-out of electron carriers to explain the sign reversal of the Hall effect in our HOPG-GW sample [32]. This effect comes from carrier localization by impurity centers due a decrease in the screening radius of the local potential induced by the magnetic field. Though the carrier freezing-out is a well-known effect in narrow band-gap semiconductors [61], it is doubtful that it can be relevant in graphite in the range of fields applied in our study [62].

The effect of As implantation is large in the Hall resistivity, contrasting with the small changes induced in the resistivity and magneto-resistance. However, the effect is qualitatively the same. For a fixed value of the applied field, increasing the impurity concentration up to As 5 at% produces a corresponding increase in the Hall resistivity. Then, similarly to observations in the MR measurements shown in Fig. 2(c), ρ_{xy} remains constant with further increase of the concentration up to As 10 at%.

Implantation at low fluences is known to produce vacancy defects in HOPG [28]. Vacancies in the graphene planes are expected to act as strong scattering centers for electron carriers, thus leading to a decrease in μ_e that further enhances the difference in the numerator of Eq. (2) upon implantation. To locally preserve charge neutrality, creation of vacancies in graphite also produces additional extrinsic holes. This effect would partially restore the total carrier density, so that it could explain the fact that relatively small changes in resistivity and magneto-resistance occur in consequence of implantation in our GW-HOPG sample.

We remark that the hole density increment upon implantation is not a conventional doping effect. Indeed, one would expect that As entering as a substitute to a C atom in graphite plays as a donor impurity. According to known results, hole doping produced by implantation in HOPG seems to be rather associated to disorder

produced by irradiation than to the valence of the implanted ion with respect to that of carbon [25,63].

4. Conclusions

Systematic magneto-transport measurements were carried out in a commercial Highly Oriented Pyrolytic Graphite sample sourced by the Great Wall Company. After being studied in the pristine state, the sample was submitted to three subsequent implantations with Arsenic ions. The fluences were chosen so that the As content at the center of the implantation profile is 2.5, 5 and 10 at%. Experiments were performed after each implantation stage.

The in-plane magneto-resistance, measured in fields up to $B=9$ T and in temperatures as high as $T=12$ K, is strongly positive and its magnitude increases with fluence up to 0.5×10^{16} ion/cm^2, then saturates. Quantum Shubnikov-de Haas oscillations were observed superimposed to the MR monotonic response. Using fast Fourier transform, the SdH oscillations were analyzed so that the fundamental frequencies for electrons and holes were extracted from the data as well the effective masses for both types of carriers. The obtained values of fundamental frequencies and effective masses are in agreement with those reported in the literature. Moreover, frequencies and effective masses were found to be independent of fluence. This result indicates that the implanted As atoms do not modify the intrinsic electron and hole densities in graphite.

The Hall resistivity shows a sign reversal as a function of the field. In low applied fields, the Hall coefficient is negative, indicating dominance of the electron current. The characteristic field where the Hall sign changes to positive depends on the fluence. The amplitude of the Hall resistivity at fixed field and temperature increases with fluence up to 0.5×10^{16} ion/cm^2, then stabilizes, as in the magneto-resistance. Quantum SdH oscillations were also observed superimposed to the monotonic contribution to the Hall resistivity. Analysis of these oscillations with FFT leads to the same results as those obtained from magneto-resistance.

We interpret our magneto-transport results by proposing a scenario where an extrinsic and significant contribution to the hole density takes part in the Boltzmann-type electronic conduction. These holes have large effective masses, and transport by them occurs in the whole range of applied magnetic fields. The sign reversal of the Hall effect may then be understood as a consequence of the increasing trap of electron carriers into Landau levels as the field magnitude is augmented. Arsenic implantation plays the role of a disorder inducer that reduces the electron mobility and generates some enlargement in the extrinsic hole density.

As a general conclusion, our results strongly suggest that As-implantation does not produce doping in the usual sense. In contrast to expectations from the semiconductor theory, according to which As should act as a donor impurity, implantation in graphite mostly affects the hole concentration as a consequence of disorder rather than of atomic substitution.

Acknowledgments

We acknowledge the partial financial support from the Brazilian agencies Fundação de Amparo à Pesquisa do Estado do Rio Grande do Sul (FAPERGS) under grant PRONEX 10/0009-2, Fundação de Apoio à Pesquisa do Estado de São Paulo (FAPESP), and Conselho Nacional de Desenvolvimento Científico e Tecnológico (CNPq).

References

[1] Y. Kopelevich, P. Esquinazi, Adv. Mater. 19 (2007) 4559.
[2] C.J. Charlier, P.J. Michenaud, Phys. Rev. B 46 (1992) 4531.
[3] J.D. Bernal, Proc. R. Soc. Lond. A 106 (1924) 749.
[4] H. Lipson, A.R. Stokes, Proc. R. Soc. Lond. A 181 (1942) 101.
[5] P. Wallace, Phys. Rev. 71 (1947) 622.
[6] J.C. Slonczewski, P.R. Weiss, Phys. Rev. 109 (1958) 272.
[7] D. Shoenberg, Philos. Trans. R. Soc. Lond. A 245 (1952) 1.
[8] J.W. McClure, Phys. Rev. 108 (1957) 612.
[9] S.Y. Zhou, G.H. Gweon, J. Graf, A.V. Fedorov, C.D. Spataru, R.D. Diehl, Y. Kopelevich, D.H. Lee, Steven G. Louie, A. Lanzara, Nat. Phys. 2 (2006) 595.
[10] N.D. Leyraud, C. Proust, D. LeBoeuf, J. Levallois, J.-B. Bonnemaison, R. Liang, D. A. Bonn, W.N. Hardy, L. Taillefer, Nature 447 (2007) 565.
[11] P. Stamenova, V. Krsticb, J.M.D. Coey, J. Magn. Magn. Mater. 290–291 (2005) 1402.
[12] S.B. Hubbard, T.J. Kershaw, A. Usher, A.K. Savchenko, A. Shytov, Phys. Rev. B 83 (2011) 035122.
[13] W.J. Spry, P.M. Scherer, Phys. Rev. 120 (1960) 826.
[14] S.J. Williamson, S. Foner, M.S. Dresselhaus, Phys. Rev. 140 (1965) A1429.
[15] B.A. Bernevig, T.L. Hughes, S. Raghu, D.P. Arovas, Phys. Rev. Lett. 99 (2007) 146804.
[16] H. Kempa, P. Esquinazi, Y. Kopelevich, Solid State Commun. 138 (2006) 118.
[17] Y. Kopelevich, B. Raquet, M. Goiran, W. Escoffier, R.R. da Silva, J.C. Medina Pantoja, I.A. Luk'yanchuk, A. Sinchenko, P. Monceau, Phys. Rev. Lett. 103 (2009) 116802.
[18] B. Fauqué, Z. Zhu, T. Murphy, K. Behnia, Phys. Rev. Lett. 106 (2011) 246405.
[19] Z. Zhu, H. Yang, A. Banerjee, L. Malone2, B. Fauqué, K. Behnia, J. Phys. Condens. Matter 23 (2011) 094204.
[20] H. Xia, W. Li, Y. Song, X. Yang, X. Liu, M. Zhao, Y. Xia, C. Song, T.-W. Wang, D. Zhu, J. Gong, Z. Zhu, Adv. Mater. 20 (2008) 4679.
[21] R. Höhne, P. Esquinazi, V. Heera, H. Weishart, A. Setzer, D. Spemann, J. Magn. Magn. Mat. 320 (2008) 966.
[22] M.A. Ramos, J.B. Quiquia, P. Esquinazi, A.M. Martin, A.C. Font, M.G. Hernández, Phys. Rev. B 81 (2010) 214404.
[23] Z. He, X. Yang, H. Xia, X. Zhou, M. Zhao, Y. Song, T. Wang, Carbon 49 (2011) 1931.
[24] N. Shukla, M. Sarkar, N. Banerji, A.K. Gupta, H.C. Verma, Carbon 50 (2012) 1817.
[25] W.K. Lee, J. Kim, C.E. Lee, J. Korean Phys. Soc. 59 (2011) 2959.
[26] Y. Wang, P. Pochet, C.A. Jenkins, E. Arenholz, G. Bukalis, S. Gemming, M. Helm, S. Zhou, Phys. Rev. B 90 (2014) 214435.
[27] O.V. Yazyev, L. Helm, Phys. Rev. B 75 (2007) 125408.
[28] X. Yang, H. Xia, X. Qin, W. Lia, Y. Daia, X. Liu, M. Zhao, Y. Xia, S. Yan, B. Wang, Carbon 47 (2009) 1399.
[29] R.F. Pires, P. Pureur, M. Behar, J.L. Pimentel Jr, J. Schaf, Y. Kopelevich, J. Appl. Phys. 111 (2012) 093922.
[30] L.M. Lifshitz, M.A. Kosevich, Sov. Phys. JETP 2 (1956) 636.
[31] B.C. Camargo, Y. Kopelevich, A. Usher, S.B. Hubbard, Appl. Phys. Lett. 108 (2016) 031604.
[32] N.B. Brandt, S.M. Chudinov, Ya. G. Ponomarev, I. Semimetals, Graphite and Its Compounds, Elsevier, Amsterdam, 1988.
[33] E. Koren, A.W. Knoll, E. Lörtscher, U. Duerig, Appl. Phys. Lett. 105 (2014) 123112.
[34] J.F. Ziegler, M.D. Ziegler, J.P. Biersack, Nucl. Instrum. Methods B 268 (2010) 1818.
[35] N. Garcia, P. Esquinazi, J.B. Quiquia, S. Dusari, New J. Phys. 14 (2012) 053015.
[36] B.T. Kelly, Physics of Graphite, Applied Science Publishers, London, 1981.
[37] S. Mrozowski, Carbon 9 (1971) 97.
[38] Y. Kopelevich, J.H.S. Torres, R.R. da Silva, F. Mrowka, H. Kempa, P. Esquinazi, Phys. Rev. Lett. 90 (2003) 156402.
[39] P.B. Alers, R.T. Webber, Phys. Rev. 91 (1953) 1060.
[40] J.H. Mangez, J.P. Issi, J. Heremans, Phys. Rev. B 14 (1976) 4381.
[41] J. Wanga, G. Cao, Y. Li, Mater. Res. Bull. 38 (2003) 1645.
[42] F.Y. Yang, K. Liu, K. Hong, D.H. Reich, P.C. Searson, C.L. Chien, Science 284 (1999) 1335.
[43] T. Liang, Q. Gibson, M.N. Ali, M. Liu, R.J. Cava, N.P. Ong, Nat. Mater. 14 (2015) 280.
[44] L.P. He, X.C. Hong, J.K. Dong, J. Pan, Z. Zhang, J. Zhang, S.Y. Li, Phys. Rev. Lett. 113 (2014) 246402.
[45] C. Shekhar, A.K. Nayak, Y. Sun, M. Schmidt, M. Nicklas, I. Leermakers, U. Zeitler, Y. Skourski, J. Wosnitza, Z. Liu, Y. Chen, W. Schnelle, H. Borrmann, Y. Grin, C. Felser, B. Yan, Nat. Phys. 11 (2015) 645.
[46] M.N. Ali, J. Xiong, S. Flynn, J. Tao, Q.D. Gibson, L.M. Schoop, T. Liang, N. Haldolaarachchige, M. Hirschberger, N.P. Ong, R.J. Cava, Nature 514 (2014) 205.
[47] Z.M. Wang, Q.Y. Xu, G. Ni, Y.W. Du, Phys. Lett. A 314 (2003) 328.
[48] Y. Kopelevich, R.R. da Silva, B.C. Camargo, A.S. Alexandrov, J. Phys. Condens. Matter 25 (2013) 466004.
[49] K. Sugihara, S. Ono, J. Phys. Soc. Jpn. 21 (1966) 631.
[50] J.A. Woollam, Phys. Rev. B 3 (1971) 4.
[51] R.B. Dingle, Proc. R. Soc. Lond. A 211 (1952) 517.
[52] L. Onsager, Philos. Mag. 43 (1952) 1006.
[53] D.E. Soule, Phys. Rev. 112 (1958) 698.
[54] Y. Kopelevich, J.C. Medina Pantoja, R.R. da Silva, F. Mrowka, P. Esquinazi, Phys.

Lett. A 355 (2006) 233.
[55] A.N. Ramanayaka, R.G. Mani, Phys. Rev. B 82 (2010) 165327.
[56] P. Esquinazi, J. Krüger, J. Barzola-Quiquia, R. Schönemann, T. Herrmansdörfer, N. Garcia, AIP Adv. 4 (2014) 117121.
[57] C.M. Hurd, The Hall Effect in Metals and Alloys, Plenum, New York, 1970.
[58] L.I. Spain, Carbon 7 (1979) 209.
[59] J.A. Woollam, Phys. Rev. Lett. 25 (1970) 810.
[60] B.S. Elman, M.S. Dresselhaus, G. Dresselhaus, E.W. Maby, H. Mazurek, Phys. Rev. B 24 (1981) 1027.
[61] M.I. Dyakonov, A.L. Efros, D.L. Mitchell, Phys. Rev. 180 (1969) 813.
[62] N.B. Brandt, G.A. Kapustin, V.G. Karavaev, A.S. Kotosonov, E.A. Svistova, Sov. Phys. JETP 40 (1974) 564.
[63] G.R. Hennig, Acceptor and donor impurities in graphite, in: Proceedings of the Fourth Conference on Carbon, Pergamon Press, 1960, p. 221.